



## Tool Length-Dependent Stability Surfaces

Tony L. Schmitz , Timothy J. Burns , John C. Ziegert , Brian Dutterer & W. R. Winfough

To cite this article: Tony L. Schmitz , Timothy J. Burns , John C. Ziegert , Brian Dutterer & W. R. Winfough (2004) Tool Length-Dependent Stability Surfaces, Machining Science and Technology, 8:3, 377-397, DOI: [10.1081/MST-200038989](https://doi.org/10.1081/MST-200038989)

To link to this article: <http://dx.doi.org/10.1081/MST-200038989>



Published online: 17 Aug 2006.



Submit your article to this journal [↗](#)



Article views: 102



View related articles [↗](#)



Citing articles: 13 View citing articles [↗](#)

## Tool Length-Dependent Stability Surfaces

Tony L. Schmitz,<sup>1,\*</sup> Timothy J. Burns,<sup>2</sup> John C. Ziegert,<sup>1</sup>  
Brian Dutterer,<sup>3</sup> and W. R. Winfough<sup>4</sup>

<sup>1</sup>Department of Mechanical and Aerospace Engineering,  
University of Florida, Gainesville, Florida, USA

<sup>2</sup>Mathematical and Computational Sciences Division and

<sup>3</sup>Fabrication Technology Division, National Institute of Standards and  
Technology, Gaithersburg, Maryland, USA

<sup>4</sup>Bourne and Koch Machine Tool Co., Rockford, Illinois, USA

### ABSTRACT

This article describes the development of three-dimensional stability surfaces, or maps, that combine the traditional dependence of allowable (chatter-free) chip width on spindle speed with the inherent dependence on tool overhang length, due to the corresponding changes in the system dynamics with overhang. The tool point frequency response, which is required as input to existing stability lobe calculations, is determined analytically using Receptance Coupling Substructure Analysis (RCSA). In this method, a model of the tool, which includes overhang length as a variable, is coupled to an experimental measurement of the holder/spindle substructure through empirical connection parameters. The assembly frequency response at the tool point can then be predicted for variations in tool overhang length. Using the graphs developed in this study, the technique of *tool tuning*, described previously in the literature, can then be carried out to select a tool overhang length for maximized material removal rate. Experimental results for both frequency response predictions and milling stability are presented.

---

\*Correspondence: Tony L. Schmitz, Department of Mechanical and Aerospace Engineering, University of Florida, Gainesville, FL 32611, USA; Fax: 352 392 1071; E-mail: tschmitz@ufl.edu.

*Key Words:* Milling; Stability; Tool tuning; Receptance coupling.

## INTRODUCTION

Research in the area of milling stability has enjoyed a rich history. Taylor recognized the process limitations imposed by chatter, as well as the complexity in modeling its source, as early as 1906 when he stated that chatter is the “most obscure and delicate of all problems facing the machinist” (Taylor, 1907). Later, work by Arnold proposed the *negative damping effect* as the source of chatter, (Arnold, 1946) while research by Tlustý and Tobias led to a fundamental understanding of *regeneration of waviness*, or the overcutting of a machined surface by a vibrating cutter, as a primary feedback mechanism for the growth of self-excited vibrations (or chatter) due to the modulation of the instantaneous chip thickness, cutting force variation, and subsequent tool vibration (Koenisberger and Tlustý, 1967; Tlustý and Polocek, 1963; Tobias, 1965; Tobias and Fishwick, 1958a, 1958b). Tlustý and Tobias also described the *mode coupling effect* as a second chatter mechanism.

Efforts at modeling the process dynamics in order to select stable combinations of chip width, or axial depth of cut in peripheral milling operations, and spindle speed, can be loosely divided into (1) analytical; and (2) numerical techniques (Altintas and Budak, 1995; Balachandran, 2001; Bayly et al., 2001, 2002; Budak and Altintas, 1998; Corpus and Endres, 2000; Davies and Balachandran, 2000; Fofana and Bukkapatnam, 2001; Grabec, 1988; Hanna and Tobias, 1974; Insperger and Stépán, 2002; Jensen and Shin, 1999; Kalmar-Nagy et al., 1999; Kegg, 1965; Merrit, 1965; Minis et al., 1990; Nayfeh et al., 1997; Pratt et al., 1999; Roa and Shin, 1999; Shridar et al., 1968; Smith and Tlustý, 1990, 1991; Stépán, 1989; Stépán and Kalmar-Nagy, 1997; Tlustý, 1985; Tlustý et al., 1983). The most common output of these simulations is the stability lobe diagram, (Koenisberger and Tlustý, 1967; Merrit, 1965; Tobias, 1965), a graphical tool which identifies the boundary between stable and unstable cutting zones in a two-dimensional map of the primary control parameters: chip width,  $b$ , and spindle speed,  $\Omega$ . Traditionally, spindle speed is varied along the abscissa (horizontal axis) and chip width along the ordinate (vertical axis). The peaks of the intersecting lobes occur approximately at spindle speeds where the tooth passing frequency is equal to an integer fraction of the natural frequency corresponding to the most flexible mode; these best spindle speeds can be estimated using Eq. (1), where  $f_n$  is the natural frequency in Hz,  $m$  is the number of teeth on the cutter,  $j$  is an integer ( $j = 1, 2, 3 \dots$ ), and  $\Omega$  is expressed in rev/min, or rpm. It should also be noted that an analog to the stability lobe diagram, the peak-to-peak or PTP diagram which identifies stability boundaries by abrupt discontinuities in the predicted peak-to-peak tool vibration or cutting force values, can be developed using time-domain numerical integration techniques (Smith and Tlustý, 1993).

$$\Omega = \frac{60f_n}{j \cdot m} \quad (1)$$



In general, stability lobe diagrams are developed by selecting the cutting parameters, which include the process-dependent specific cutting energy coefficients, radial immersion, and system dynamics (often selected as the tool point frequency response, although the workpiece dynamics must also be considered in some instances), then carrying out the selected simulation algorithm. In this case, the system dynamics are considered to be fixed and a new set of stability calculations must be completed if the system changes.

### TOOL TUNING

Recent research by Davies et al. (1998), Smith et al. (1998), Tlustý et al. (1996) has suggested that, rather than assuming fixed dynamics, the tool point frequency response can be varied by adjusting the tool overhang length in a method referred to as *tool tuning*. In this case, improved material removal rates can be obtained by (1) shifting the natural frequency corresponding to the most flexible mode (often the fundamental tool vibrational mode) and, therefore, the location of the peaks of the stability lobes as shown in Eq. (1), e.g., adjusting the tool length to move a lobe peak to the top available spindle speed; and/or (2) varying the tool length in order to obtain an overlap between the fundamental tool natural frequency and one of the spindle natural frequencies. This results in the *dynamic absorber effect* (Schmitz and Donaldson, 2000) where the matched natural frequencies lead to a dynamically stiffer system, similar to the result observed when adding the classic Frahm dynamic absorber (Den Hartog, 1956) to a base structure in order to attenuate vibration at a particular excitation frequency.

### RECEPTANCE COUPLING SUBSTRUCTURE ANALYSIS

#### Method Description

In order to analytically determine the tool point frequency response as a function of tool length and apply the method of tool tuning, the Receptance Coupling Substructure Analysis (RCSA) method was developed (Schmitz, 2000; Schmitz and Davies, 2001; Schmitz et al., 2001). In this technique, based on earlier receptance coupling work by Bishop and Johnson (1960), Duncan (1947), and, later, Ferreira and Ewins (1995), an experimental measurement of the holder/spindle substructure, or component, is coupled to an analytical model of the tool through two empirical complex stiffness vectors, which include linear and rotational stiffness and viscous damping terms that characterize the nonrigid behavior of the connection between the holder and tool (e.g., thermal shrink fit, collet, or elastic deformation interference fit [<http://www.schunk-usa.com/hmhs/home.html>]). The primary benefit of using receptance, rather than modal, coupling for this application is that no restrictions are placed on the number of modes included in either the holder/spindle experimental measurements or tool model and the holder/spindle frequency response data can be used directly without requiring a modal fit. Since the desired output is



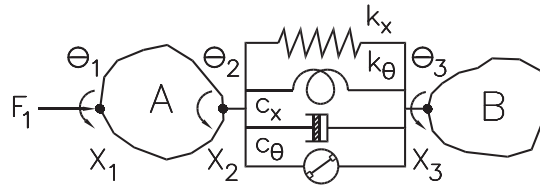


Figure 1. RCSA holder/spindle/tool model including connection parameters.

the tool point frequency response, the most straightforward approach is to directly couple component receptance terms and avoid the modal fitting step all together.

The model for the coupling between the holder/spindle and tool components is shown in Fig. 1. There are three translational and three rotational assembly coordinates identified, with spatial positions coincident with the coupling locations (coordinates  $X_2/\Theta_2$  on the tool and  $X_3/\Theta_3$  on the holder/spindle component) and the point of interest (coordinates  $X_1/\Theta_1$  at the free end of tool). The connection between  $X_2/\Theta_2$  and  $X_3/\Theta_3$  is composed of a linear spring,  $k_x$ , torsional spring,  $k_\theta$ , linear viscous damper,  $c_x$ , and rotational viscous damper,  $c_\theta$ . In order to determine the assembly direct, or driving point, frequency response at the tool point,  $G_{11}(\omega) = X_1(\omega)/F_1(\omega)$ , which is used as input to the selected process stability simulation, the following steps must be completed:

- (a) Use impact testing to measure the holder/spindle component (i.e., no tool inserted in holder) frequency response function (FRF),  $H_{33} = X_3/F_3$ , at the free end in two orthogonal directions in the plane of the cut, i.e., perpendicular to the spindle centerline. Typically, the measurement directions are selected to be coincident with the feed directions of the machine tool. Here, we neglect potential contributions of the tool/holder/spindle assembly axial frequency response to the occurrence of chatter, although Altintas has suggested that the axial response can be considered in a three-dimensional, or 3-D, chatter model (Altintas, 2001).
- (b) Develop an analytic model of the free-free tool using the closed form receptance terms, which capture both the rigid body and transverse vibration behavior of the tool, developed by Bishop and Johnson (1960). We have selected to treat the tool as an Euler-Bernoulli beam with a constant cross-section, which requires that an effective diameter,  $d_{\text{eff}}$ , be determined for calculation of the 2nd area moment of inertia,  $I = \pi d_{\text{eff}}^4/64$ . The effective diameter is based on the tool overhang length,  $L$ , total length,  $L_T$ , tool material density,  $\rho$ , shank diameter,  $d$ , and tool mass,  $M$ . See Eq. (2). Fundamentally, this equation calculates the diameter of a uniform cross-section beam with (1) a mass equal to the difference between the total tool mass and the mass of the tool shank inside the holder; and (2) a length equal to the overhang length of the tool, given the tool material density.

$$d_{\text{eff}} = \sqrt[4]{\frac{4M - \pi\rho d^2(L_T - L)}{\pi\rho L}} \quad (2)$$



We have also added structural, or hysteretic, damping to the tool model by replacing Young's elastic modulus,  $E$ , for the tool material with the complex modulus,  $E' = (1 + i\eta)E$ , where  $\eta$  is the structural damping factor, a small dimensionless constant. This modifies the frequency-dependent term  $\lambda = (\omega^2 m/EI)^{1/4}$  from Bishop and Johnson (1960) to be  $\lambda' = (\omega^2 m/[(1 + i\eta)EI])^{1/4} = \lambda/(1 + i\eta)^{1/4} \approx \lambda(1 - i(\eta/4))$ . To simplify notation, we drop the primes from  $E'$  and  $\lambda'$  in the expressions shown in Eq. (3), which define the required free-free tool component receptance terms. In these expressions, different designations have been applied to the four receptance types found in our model, specifically,  $H_{ij} = x_i/f_j$ ,  $L_{ij} = x_i/m_j$ ,  $N_{ij} = \theta_i/f_j$ , and  $P_{ij} = \theta_i/m_j$ .

$$\begin{aligned} \frac{x_1}{f_1}(\omega) = H_{11} &= \frac{-(\cos L\lambda \cdot \sinh L\lambda - \sin L\lambda \cdot \cosh L\lambda)}{\lambda^3 EI(\cos L\lambda \cdot \cosh L\lambda - 1)} \\ \frac{x_2}{f_2}(\omega) = H_{22} &= H_{11} \\ \frac{x_2}{m_2}(\omega) = L_{22} &= \frac{\sin L\lambda \cdot \sinh L\lambda}{\lambda^2 EI(\cos L\lambda \cdot \cosh L\lambda - 1)} \quad \frac{\theta_2}{f_2}(\omega) = N_{22} = L_{22} \\ \frac{\theta_2}{m_2}(\omega) = P_{22} &= \frac{\cos L\lambda \cdot \sinh L\lambda + \sin L\lambda \cdot \cosh L\lambda}{\lambda EI(\cos L\lambda \cdot \cosh L\lambda - 1)} \\ \frac{x_1}{f_2}(\omega) = H_{12} &= \frac{\sin L\lambda - \sinh L\lambda}{\lambda^3 EI(\cos L\lambda \cdot \cosh L\lambda - 1)} \quad \frac{x_2}{f_1}(\omega) = H_{21} = H_{12} \\ \frac{x_1}{m_2}(\omega) = L_{12} &= \frac{\cos L\lambda - \cosh L\lambda}{\lambda^2 EI(\cos L\lambda \cdot \cosh L\lambda - 1)} \quad \frac{\theta_2}{f_1}(\omega) = N_{21} = L_{12} \end{aligned} \tag{3}$$

- (c) Measure the tool point response for the assembly in one direction at a known overhang. This data allows the determination of the connection parameters,  $k_x, k_\theta, c_x$ , and  $c_\theta$ , by nonlinear least squares best fit. Clearly, an *a priori* determination of these values without the requirement of an experimental measurement and fit is the preferred solution and will be the subject of future investigations. However, the empirical determination of these parameters still allows the model shown in Fig. 1 to be developed and analytic prediction of FRFs to be completed for variation in tool overhang length. In this work, once a set of connection parameters  $\{k_x, k_\theta, c_x, \text{ and } c_\theta\}$  was determined from the fit to a single tool point measurement, the same values were used for all subsequent predictions. This use of constant connection parameters is shown to be sufficient for the range of tool lengths shown here.

### Mathematical Derivation

If harmonic external excitations of force  $F(t) = Fe^{i\omega t}$  and/or moment  $M(t) = Me^{i\omega t}$  are applied to the assembly shown in Fig. 1, the resulting displacements



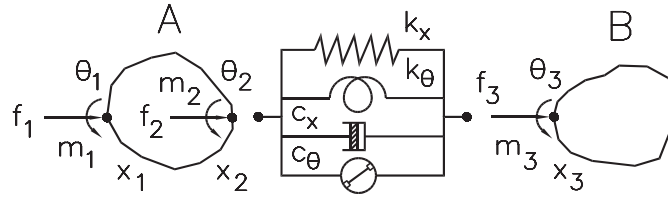


Figure 2. Component forces and moments due to force  $F_1(t)$ .

and rotations can be written as  $X(t) = Xe^{i\omega t}$  and  $\Theta(t) = \Theta e^{i\omega t}$ , respectively. In order to determine an analytical expression for the tool point frequency response  $G_{11}(\omega)$ , we apply the harmonic force  $F_1(t)$  to coordinate  $X_1$  of the assembly. The resulting forces/moments and displacements/rotations for the individual components, represented in Fig. 2, can then be expressed as shown in Eq. (4). The equilibrium conditions for this loading condition are shown in Eq. (5); the compatibility conditions are provided in Eq. (6). The latter conditions serve two purposes: (1) they define the relationship between the two component displacements/rotations and forces/moments; and (2) they specify that the component coordinates are at the same spatial locations as the assembly coordinates.

$$\begin{aligned}
 x_1 &= H_{11}f_1 + H_{12}f_2 + L_{12}m_2 \\
 \theta_1 &= N_{11}f_1 + N_{12}f_2 + P_{12}m_2 \\
 x_2 &= H_{21}f_1 + H_{22}f_2 + L_{22}m_2 \\
 \theta_2 &= N_{21}f_1 + N_{22}f_2 + P_{22}m_2 \\
 x_3 &= H_{33}f_3 + L_{33}m_3 \\
 \theta_3 &= N_{33}f_3 + P_{33}m_3
 \end{aligned} \tag{4}$$

$$\begin{aligned}
 f_1 &= F_1 \\
 f_2 + f_3 &= 0 \\
 m_2 + m_3 &= 0
 \end{aligned} \tag{5}$$

$$\begin{aligned}
 k_x(x_3 - x_2) + c_x(\dot{x}_3 - \dot{x}_2) &= f_2 = -f_3 \\
 k_\theta(\theta_3 - \theta_2) + c_\theta(\dot{\theta}_3 - \dot{\theta}_2) &= m_2 = -m_3 \\
 x_1 &= X_1, \quad x_2 = X_2, \quad x_3 = X_3 \\
 \theta_1 &= \Theta_1, \quad \theta_2 = \Theta_2, \quad \theta_3 = \Theta_3
 \end{aligned} \tag{6}$$

Because we have assumed harmonic motion (due to harmonic excitation), the time derivative terms in Eq. (6) can be rewritten in the form  $\dot{x}(t) = i\omega X e^{i\omega t}$  and  $\dot{\theta}(t) = i\omega \Theta e^{i\omega t}$ . Substitution in Eq. (6) yields Eq. (7). To simplify notation, we now define the complex, frequency dependent stiffness terms  $K_x = k_x + i\omega c_x$  and  $K_\theta = k_\theta + i\omega c_\theta$ .

$$\begin{aligned}
 k_x(x_3 - x_2) + c_x(\dot{x}_3 - \dot{x}_2) &= (k_x + i\omega c_x)(x_3 - x_2) = K_x(x_3 - x_2) = f_2 = -f_3 \\
 k_\theta(\theta_3 - \theta_2) + c_\theta(\dot{\theta}_3 - \dot{\theta}_2) &= (k_\theta + i\omega c_\theta)(\theta_3 - \theta_2) = K_\theta(\theta_3 - \theta_2) = m_2 = -m_3
 \end{aligned} \tag{7}$$



**Tool Length-Dependent Stability Surfaces**

To determine  $G_{11}(\omega)$ , we first substitute the component displacements and rotations defined in Eq. (4) into Eq. (7). This result is shown in Eq. (8). In Eq. (9), this equation has been expressed in matrix form.

$$\begin{aligned}
 K_x(H_{33} + H_{22})f_3 + K_x(L_{33} + L_{22})m_3 - K_xH_{21}f_1 &= -f_3 \\
 K_\theta(N_{33} + N_{22})f_3 + K_\theta(P_{33} + P_{22})m_3 - K_\theta N_{21}f_1 &= -m_3
 \end{aligned} \tag{8}$$

$$\begin{aligned}
 \begin{bmatrix} K_x(H_{33} + H_{22}) + 1 & K_x(L_{33} + L_{22}) \\ K_\theta(N_{33} + N_{22}) & K_\theta(P_{33} + P_{22}) + 1 \end{bmatrix} \begin{Bmatrix} f_3 \\ m_3 \end{Bmatrix} &= [A] \begin{Bmatrix} f_3 \\ m_3 \end{Bmatrix} \\
 &= \begin{bmatrix} K_xH_{21} \\ K_\theta N_{21} \end{bmatrix} \begin{Bmatrix} f_1 \\ f_1 \end{Bmatrix}
 \end{aligned} \tag{9}$$

We can now make the substitution  $f_1 = F_1$  from the equilibrium conditions and solve Eq. (9) for  $\{f_3 \ m_3\}^T$  as shown in Eq. (10).

$$\begin{Bmatrix} f_3 \\ m_3 \end{Bmatrix} = [A]^{-1} \begin{bmatrix} K_xH_{21} \\ K_\theta N_{21} \end{bmatrix} \begin{Bmatrix} F_1 \\ F_1 \end{Bmatrix} \tag{10}$$

The relationships between the tool component displacement and rotation at coordinate 1,  $x_1$ , and  $\theta_1$ , and the component forces,  $f_1$  and  $f_2$ , and moment,  $m_2$ , were expressed in Eq. (4). These can be rewritten in matrix form as shown in Eq. (11). Substitution of  $x_1 = X_1$ ,  $\theta_1 = \Theta_1$ ,  $f_1 = F_1$ ,  $f_2 = -f_3$ ,  $m_2 = -m_3$ , and the result from Eq. (10) in Eq. (11) yields Eq. (12).

$$\begin{Bmatrix} x_1 \\ \theta_1 \end{Bmatrix} = \begin{bmatrix} H_{11} \\ N_{11} \end{bmatrix} \begin{Bmatrix} f_1 \\ f_1 \end{Bmatrix} + \begin{bmatrix} H_{12} & L_{12} \\ N_{12} & P_{12} \end{bmatrix} \begin{Bmatrix} f_2 \\ m_2 \end{Bmatrix} \tag{11}$$

$$\begin{Bmatrix} X_1 \\ \Theta_1 \end{Bmatrix} = \begin{bmatrix} H_{11} \\ N_{11} \end{bmatrix} \begin{Bmatrix} F_1 \\ F_1 \end{Bmatrix} - \begin{bmatrix} H_{12} & L_{12} \\ N_{12} & P_{12} \end{bmatrix} [A]^{-1} \begin{bmatrix} K_xH_{21} \\ K_\theta N_{21} \end{bmatrix} \begin{Bmatrix} F_1 \\ F_1 \end{Bmatrix} \tag{12}$$

where

$$[A]^{-1} = \frac{1}{\det A} \begin{bmatrix} K_\theta(P_{33} + P_{22}) + 1 & -K_x(L_{33} + L_{22}) \\ -K_\theta(N_{33} + N_{22}) & K_x(H_{33} + H_{22}) + 1 \end{bmatrix}$$

and

$$\det A = (K_x(H_{33} + H_{22}) + 1)(K_\theta(P_{33} + P_{22}) + 1) - K_x(L_{33} + L_{22})K_\theta(N_{33} + N_{22})$$

The desired assembly receptance term  $G_{11}(\omega)$  can now be determined from the top row in Eq. (12). This result is shown in Eq. (13). The receptance  $G_{41}(\omega) = \Theta_1/F_1$  is also available from the second row of Eq. (12). Although we are only interested in determining the assembly direct displacement to force frequency response at the tool point, the full receptance matrix (shown in Eq. (14)) can be populated using this method.

$$\begin{aligned}
 G_{11}(\omega) &= \frac{X_1}{F_1} \\
 &= H_{11} - \frac{H_{12}}{\det A} [K_xH_{21}(K_\theta(P_{33} + P_{22}) + 1) - K_\theta N_{21}K_x(L_{33} + L_{22})]
 \end{aligned} \tag{13}$$





$$-\frac{L_{12}}{\det A} [K_{\theta} N_{21} (K_x (H_{33} + H_{22}) + 1) - K_x H_{21} K_{\theta} (N_{33} + N_{22})]$$

$$\begin{pmatrix} X_1 \\ X_2 \\ X_3 \\ \Theta_1 \\ \Theta_2 \\ \Theta_3 \end{pmatrix} = \begin{bmatrix} G_{11} & G_{12} & G_{13} & G_{14} & G_{15} & G_{16} \\ G_{21} & G_{22} & G_{23} & G_{24} & G_{25} & G_{26} \\ G_{31} & G_{32} & G_{33} & G_{34} & G_{35} & G_{36} \\ G_{41} & G_{42} & G_{43} & G_{44} & G_{45} & G_{46} \\ G_{51} & G_{52} & G_{53} & G_{54} & G_{55} & G_{56} \\ G_{61} & G_{62} & G_{63} & G_{64} & G_{65} & G_{66} \end{bmatrix} \begin{pmatrix} F_1 \\ F_2 \\ F_3 \\ M_1 \\ M_2 \\ M_3 \end{pmatrix} \quad (14)$$

Equation 13 expresses the tool point frequency response as a function of the tool analytic receptances identified in Eq. (3), the measured holder/spindle direct FRF<sup>a</sup>  $H_{33}$ , and the complex stiffnesses  $K_x$  and  $K_{\theta}$ , all of which can be obtained by following the three steps (a), (b), and (c) described in the “Method Description” section. However, this equation also contains the holder/spindle component receptances  $L_{33} = x_3/m_3$ ,  $N_{33} = \theta_3/f_3$ , and  $P_{33} = \theta_3/m_3$ . Although it would be possible to use a pair of linear transducers (e.g., accelerometers) located a known distance apart to measure the rotation at the free end of the holder/spindle due to an impact force and obtain  $N_{33}$ , the remaining two terms are more problematic due to the physical difficulty in applying an impulsive moment to the structure without adding complexity to the measurement process; note that a primary goal of the RCSA method is to minimize the number of measurements required to construct the assembly model. Of course, if symmetry of the holder/spindle component receptance matrix is assumed,  $L_{33}$  could be set equal to the  $N_{33}$  result. However,  $P_{33}$  must still be obtained by yet another measurement.

In this work, we have assumed that  $L_{33}$ ,  $N_{33}$ , and  $P_{33}$  are equal to zero in the absence of reliable measurement techniques. Although this may appear to be an unrealistic assumption, it can be shown that these terms play a small role in the prediction of  $G_{11}$  for typical tool/holder/spindle assemblies, where the holder/spindle frequency response has significantly higher dynamic stiffness than the tool response (Schmitz and Burns, 2003). This assertion is supported by the good agreement between the measured and predicted tool point FRFs shown in the “FRF Variation with Overhang Changes” section.

### 3-D STABILITY SURFACE DEVELOPMENT

In this section, we describe the development of tool overhang length-dependent stability surfaces that include the traditional two-dimensional map of spindle speed vs. limiting chip width, as well as a third axis for variations in tool overhang length. RCSA was applied to a given tool/holder/spindle system in order to develop the

<sup>a</sup>Because there is some portion of the tool mass inside the holder, we actually perform receptance coupling twice. First, the tool mass inside the holder is coupled to the holder/spindle FRF assuming a rigid connection. Then, the modified holder/spindle result is coupled to the analytic tool model using the empirical complex stiffness values.



model shown in Fig. 1. Using this model, the tool length was varied and the corresponding changes in the tool point FRF predicted. This data was then used as input to the stability analysis reported by Altintas and Budak (1995).

### FRF Variation with Overhang Changes

A tool/holder/spindle model was constructed using a two flute helical endmill, collet-type tool/holder connection, HSK-63A holder/spindle interface, and 20,000 rpm spindle. The carbide endmill was 152.4 mm long with a 12.7 mm diameter shank and had a mass of 246.8 g. The flute length was 16 mm, the shank length was 65 mm, and the neck was relieved to a diameter of 11.1 mm. An allowable overhang range of 112.5 mm (8.9:1 length to diameter, or L:D, ratio) to 124.0 mm (9.8:1) was selected. The carbide density and modulus were taken to be  $14.5 \times 10^3 \text{ kg/m}^3$  and  $5.853 \times 10^{11} \text{ N/m}^2$ , respectively (Trent and Wright, 2000). In all measurements, the collet torque was set to the manufacturer-recommended value of 61 N-m (45 ft-lb<sub>f</sub>) using a torque wrench.

Following the algorithm described in the “Method description” section, the holder was placed in the spindle and the direct FRF at the holder free end was recorded using impact testing in the vertical ( $y$ ) and horizontal ( $x$ ) directions for the horizontal spindle axis ( $z$ ) machine configuration. The  $x$  and  $y$ -direction results are shown in Fig. 3; the reader may note the asymmetry between the two directions. For the measurement bandwidth of 1600 Hz (1 Hz frequency resolution), three  $x$ -direction modes are identified here: 532, 675, and 800 Hz. Two modes at 550 and 725 Hz are identified in the  $y$ -direction. For all FRF measurements completed in this study, the instrumented hammer and low-mass accelerometer calibration constants (i.e., sensitivities) were 806 N/V and 1033 m/s<sup>2</sup>/V, respectively. The excitation bandwidth for the hammer was approximately 3 kHz and good coherence was observed for all measurements.

Next, the tool receptances were calculated for a mid-range overhang length of 118.5 mm using Eqs. (2) and (3). A structural damping factor of 0.001 was assumed for the complex modulus calculation due to the difficulty in completing free-free boundary condition FRF measurements on endmills. Finally, an  $x$ -direction tool point FRF was recorded for the tool/holder/spindle assembly and fit using Eq. (13) to determine the connection parameters and complete the RCSA model. The nonlinear least squares fit connection parameters are provided in Table 1.

Predicted results using the fit parameters in Table 1 are shown in Figs. 4 ( $x$ -direction) and 5 ( $y$ -direction). The overhang lengths are the minimum and maximum values, 112.5 and 124.0 mm, respectively, and a near mid-range value of 121.0 mm. For the full range of measurements, good agreement is observed between the measured and predicted data in both the  $x$  and  $y$ -directions.

Several observations can be made from these measurements. First, for the 112.5 mm overhang length (first column in Figs. 4 and 5), both the  $x$  and  $y$ -direction results exhibit two clear modes. For the  $x$ -direction measurement in Fig. 4, a more flexible mode is seen at 750 Hz and a stiffer mode at 817 Hz. This is due to interaction between the holder/spindle mode at 800 Hz and the clamped tool fundamental mode at 781.5 Hz. This dynamic absorber effect causes the



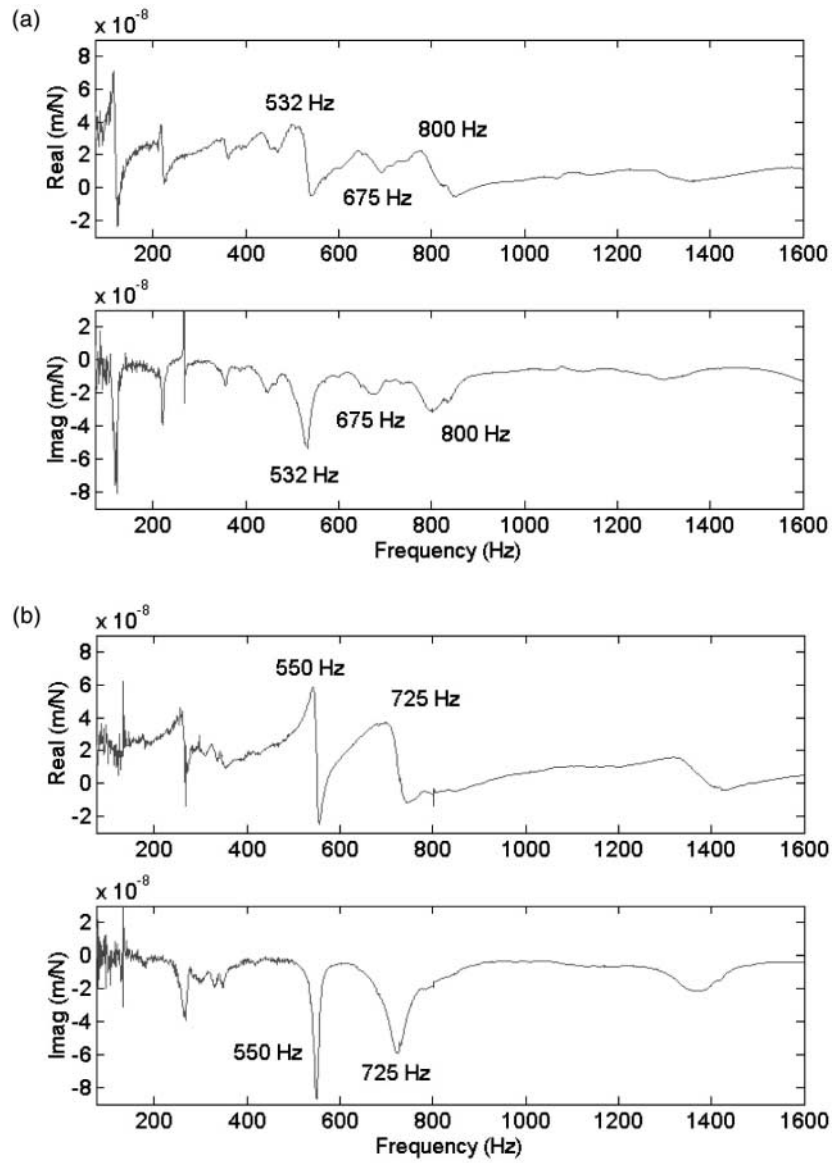


**Figure 3.** (a) Holder/spindle  $x$ -direction frequency response and (b) Holder/spindle  $y$ -direction frequency response.

**Table 1.** Nonlinear least squares fit connection parameters.

$k_x$ (N/m)	$k_\theta$ (N-m/rad)	$c_x$ (N-s/m)	$c_\theta$ (N-m-s/rad)
$6.8 \times 10^7$	$2.7 \times 10^6$	3,816	406



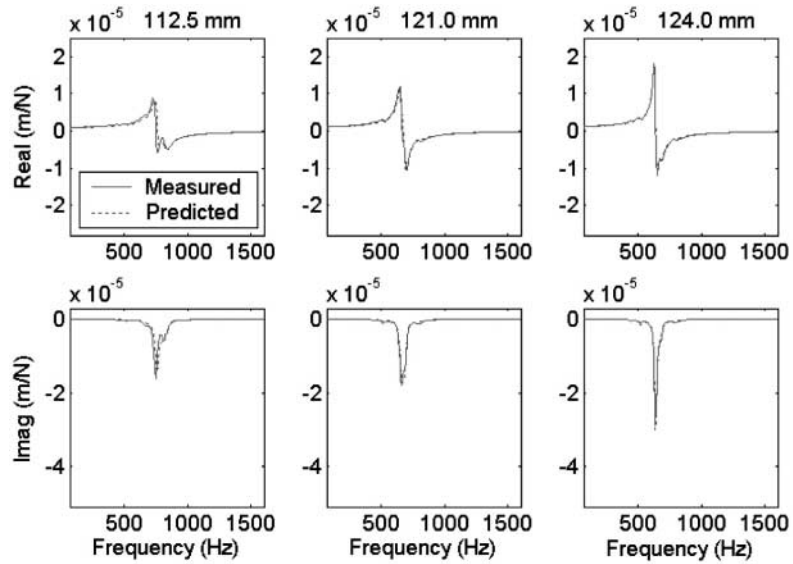


Figure 4. Assembly tool point FRF measurements and predictions for  $x$ -direction.

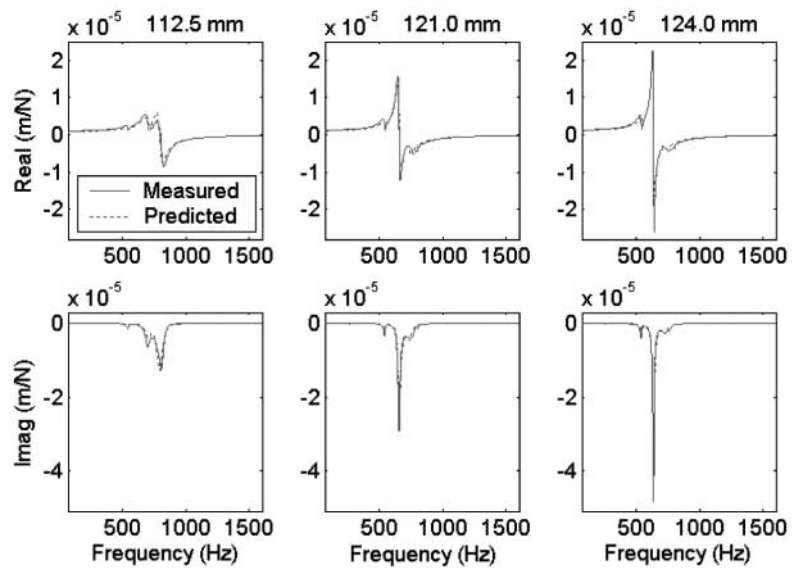
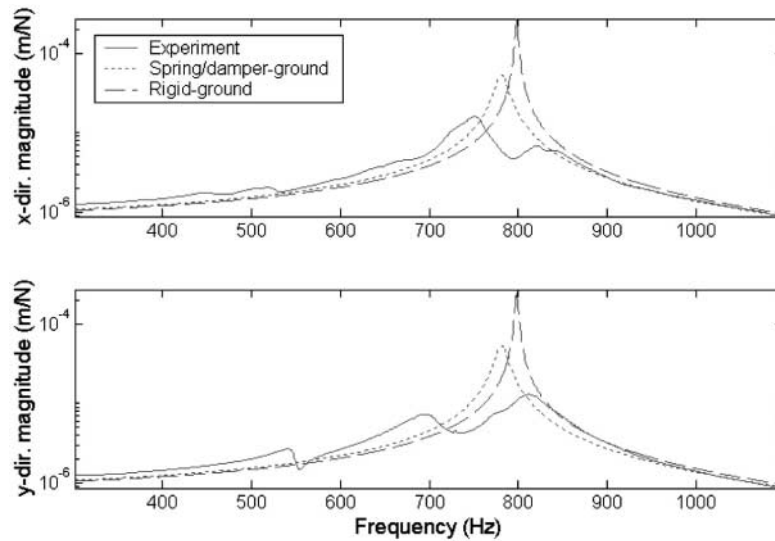


Figure 5. Assembly tool point FRF measurements and predictions for  $y$ -direction.

holder/spindle mode to be pushed to a higher natural frequency of 817 Hz and moves the tool mode down in frequency to 750 Hz. In the Fig. 5  $y$ -direction measurement, a stiffer mode is observed to the left and a more flexible mode to the right. In this case, the holder/spindle mode is located at 725 Hz (below the clamped tool natural





**Figure 6.** Comparison between cantilever tool, tool connected to ground using empirical connection parameters, and experimental results for 112.5 mm overhang length.

frequency), so it is shifted down to 702 Hz, while the tool mode is up-shifted to 809 Hz. Figure 6 shows a comparison of the same tool connected to ground (i.e., a rigid spindle) using the connection coefficients from Table 1, the tool rigidly connected to ground (i.e., infinite connection stiffness, no damping), and the experimental results from Figs. 4 and 5 (only the real parts of the FRFs are shown). A logarithmic scale in the  $y$ -axis was required to effectively capture the dramatic differences in amplitude. The cantilever response obtained from the rigid connection to ground yields the most flexible result with the highest natural frequency. When the connection stiffness and damping terms from Table 1 are used to connect the tool to ground, the natural frequency is lowered and the amplitude is decreased. However, a dynamically stiffer assembly is produced when connecting the tool to the flexible spindle due to the interaction between the tool and holder/spindle modes. These results support the conclusions of Smith et al. (1999), where the authors showed experimentally that increasing the drawbar force in high-speed spindles can reduce the system stability because, although the holder/spindle interface stiffness increases, the damping may decrease at a higher rate.

For the 121.0 mm overhang length (second column in Figs. 4 and 5), it is seen that the  $y$ -direction result is more flexible than the  $x$ -direction. In this case, the tool clamped mode falls directly between the  $y$ -direction holder/spindle modes at 550 and 725 Hz, so very little interaction occurs. In fact, it is clearly seen that the two modes bracket the more flexible tool mode in Fig. 5. For the  $x$ -direction result, however, there is an interaction between the tool mode and the 675 Hz holder/spindle mode. Similar results are observed for the 124.0 mm overhang tool, except the tool mode has now been shifted slightly to the left.



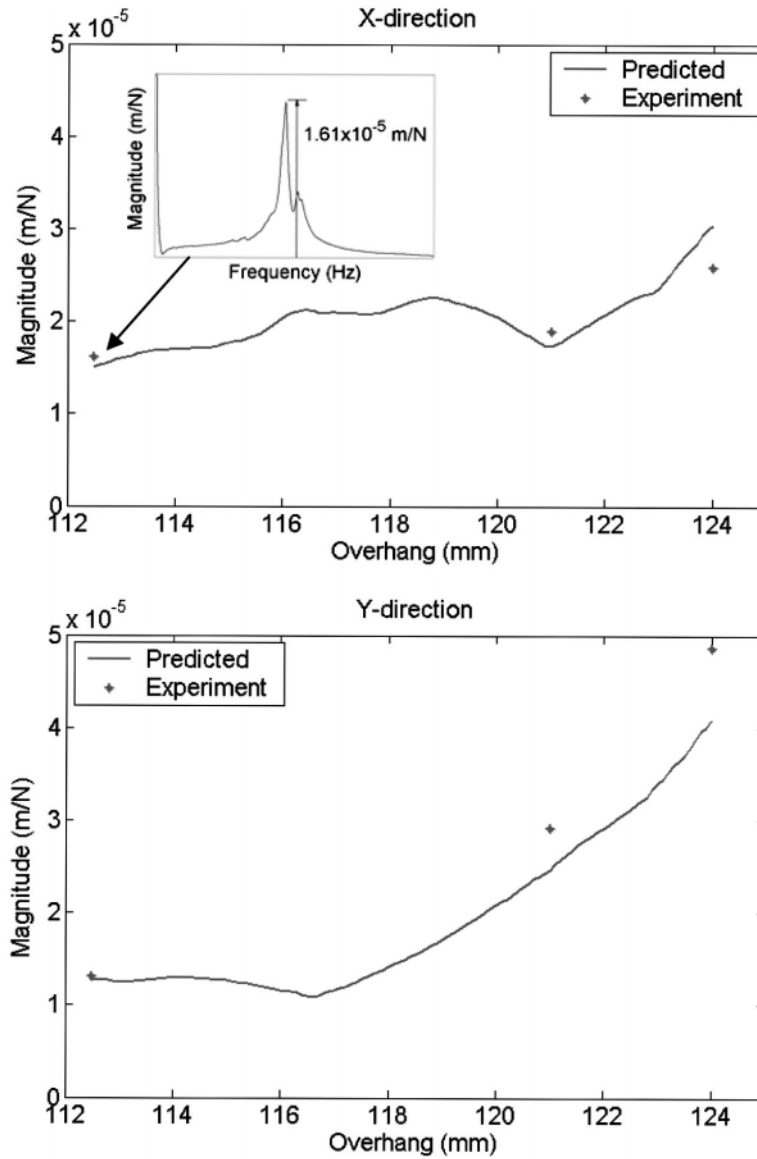


*Figure 7.* Maximum magnitude comparison for RCSA predictions (solid line) and measurements (asterisks). The top figure gives the  $x$ -direction results; the  $y$ -direction results are shown in the bottom figure.

A comparison between the experimental and predicted results is provided in Fig. 7. Here, the maximum value of the FRF magnitude within the frequency range of interest has been plotted as a function of overhang length. The predicted results are shown as a solid line and the measurement results are identified by asterisks.



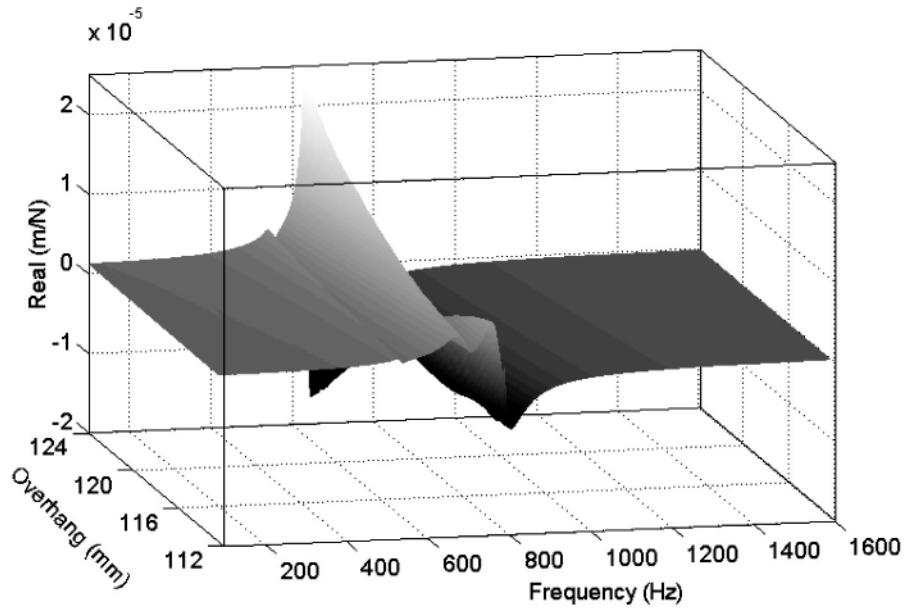


Figure 8. 3-D real part plot for 12.7 mm diameter tool from RCSA predictions.

Good agreement is observed, although the model under-predicts the amplitude for the higher overhang values in the  $y$ -direction.

Rather than plotting single overhang length FRF results, it is also possible to develop 3-D FRF graphs using the RCSA tool/holder/spindle model. Results for variation in overhang length from 112.5 to 124.0 mm in 0.1 mm increments for the  $y$ -direction predictions are shown in Fig. 8, which displays the real part of the multiple predicted FRFs. This figure shows the strong interaction between the tool mode and spindle mode at the minimum overhang length and large decrease in dynamic stiffness for the maximum overhang length.

### Stability Analysis

We have applied the stability analysis developed by Altintas and Budak (1995). This method transforms the time-dependent dynamic milling equations into a time invariant, but radial immersion-dependent system. The time varying coefficients of the dynamic milling equations, which depend on the angular orientation of the cutter as it rotates through the cut, are expanded into a Fourier series and then truncated to include only the average component. The analytic stability equations provided in reference (Altintas and Budak, 1995) have been slightly rearranged here to recast the eigenvalue problem into the form expected by MATLAB, the computing language used in this study. The *eig.m* MATLAB function expects a problem statement in the form  $\det(A - \lambda I) = 0$ , while Altintas and Budak pose the problem as  $\det$



$(I + \Lambda A) = 0$ , where  $\lambda$  and  $\Lambda$  are the system complex eigenvalues for the two formulations, respectively, and  $A$  is defined in Eq. (19). The terms  $\alpha_{xx}$ ,  $\alpha_{xy}$ ,  $\alpha_{yx}$ , and  $\alpha_{yy}$ , derived in reference (Altintas and Budak, 1995), depend on the selected starting and exit angles for the cut and the radial direction specific cutting energy coefficient,  $K_r$ . The resulting stability relationships are shown in Eqs. (20)–(22), where  $G_x$  and  $G_y$  are the system FRFs in the  $x$  and  $y$ -directions, respectively,  $K_t$  is the tangential direction specific cutting energy coefficient,  $f_c$  is the chatter frequency (in Hz) should it occur,  $N$  is the lobe number, and  $m$  is the number of cutter teeth.

$$A = \begin{bmatrix} \alpha_{xx}G_x & \alpha_{xy}G_y \\ \alpha_{xy}G_x & \alpha_{yy}G_y \end{bmatrix} \quad (15)$$

$$b_{lim} = \frac{2\pi \text{Re}(\lambda)}{mK_t(\text{Re}(\lambda)^2 + \text{Im}(\lambda)^2)} \left( 1 + \left( \frac{\text{Im}(\lambda)}{\text{Re}(\lambda)} \right)^2 \right) \quad (16)$$

$$\Omega = \frac{2\pi f_c}{m} \frac{60}{(\gamma + 2\pi N)} \quad (17)$$

$$\gamma = \pi - 2 \tan^{-1} \left( \frac{\text{Im}(\lambda)}{\text{Re}(\lambda)} \right) \quad (18)$$

This method provides a vector of  $b_{lim}$  (i.e., the limiting axial depth of cut) values which corresponds to a different spindle speed vector for each  $N$  value included in the simulation. For example, if the first five lobes are to be plotted, there will be a different spindle speed vector for each  $N$  value,  $N = 0, 1, 2, 3,$  and  $4$ . Although the output provided from the stability analysis allows a visual examination to determine best spindle speeds and corresponding  $b_{lim}$  values, in our case we require the organization of the stability information included in the multiple parameterized overlapping lobes (that make up the analytic stability lobe diagram) into a single pair of vectors that describe the continuous relationship between spindle speed and allowable chip width. In other words, we require a numerical representation of the lower boundary imposed by the convolution of the individual stability lobes (Schmitz, 2002).

The main difficulty in determining the continuous stability boundary beneath the lobes is that, although the chatter frequencies are equally spaced, the mapping of these frequencies to corresponding spindle speeds produces nonuniformly spaced data. Therefore, it is not possible to simply compare the  $b_{lim}$  values on overlapping lobes at each spindle speed to determine the minimum value. To overcome this difficulty, the individual lobes were linearly interpolated over a preselected range of equally spaced spindle speeds, e.g., 5000 rpm to 30,000 rpm. Each lobe covered only a portion of the total spindle speed range, so  $b_{lim}$  was set to an arbitrarily high value for those spindle speeds not spanned by that particular lobe. Once all lobes were mapped onto the uniformly spaced spindle speed vector, the minimum  $b_{lim}$  value from the set of interpolated lobes was selected at each spindle speed to give the final





stability boundary. In this research, we used the MATLAB *interp1.m* function to carry out the linear interpolation step.

### 3-D Stability Surfaces

The 3-D stability surface developed for the 12.7 mm diameter, two flute, carbide endmill using the Altintas and Budak formulation is shown in Fig. 9. The workpiece material was 6061-T6 aluminum ( $K_t = 700 \text{ N/mm}^2$  and  $K_r = 0.3$ ) and  $x$ -direction slotting, or 100% radial immersion, conditions were selected. It is seen that increasing the tool length decreases the limiting axial depth; the maximum allowable depth of cut is 0.95 mm at 23,190 rpm for a 112.5 mm overhang and 0.78 mm at 19,310 rpm for a 124.0 mm overhang. The associated MRR contour plot (a feed per tooth of 0.1 mm was selected) is shown in Fig. 10. Again, the maximum MRR tends to decrease with increasing overhang length. However, for a top spindle speed of 20,000 rpm, the selected overhang should be near 122 mm, rather than the minimum possible overhang length for maximized MRR. This occurs because a lobe peak has shifted to 20,000 rpm at this overhang.

To verify the utility of applying RCSA frequency response predictions to stability lobe calculation and cutting parameter selection, an overhang length of 121.0 mm (near the optimum overhang for a 20,000 rpm spindle speed from Fig. 10) was selected in simulation and stability lobes produced using the Altintas and Budak analysis. Slot machining tests were then carried out at 9 different spindle speeds from 10,000 rpm to 20,000 rpm (using a constant chip load of 0.1 mm/tooth). Chatter was identified by an evaluation of the cut surface as well as by monitoring the audio cutting signal. These results are shown in Fig. 11. Good agreement is observed.

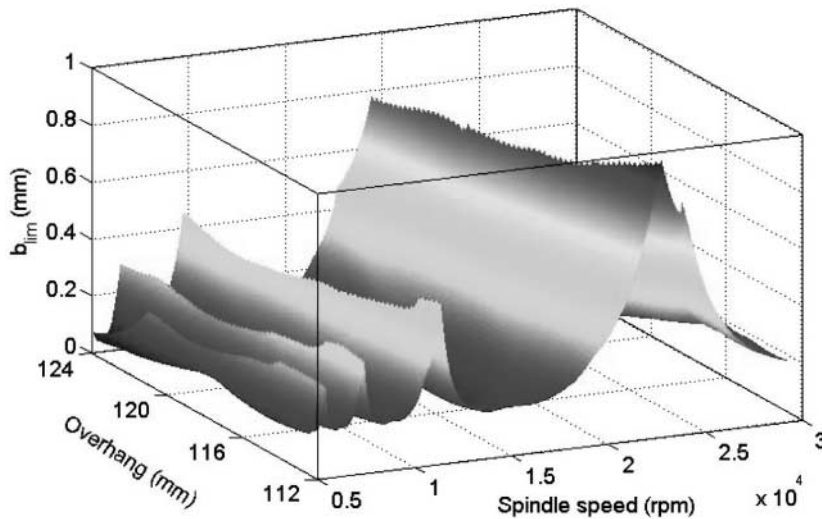


**Figure 9.** Altintas and Budak formulation 3-D stability surface for 12.7 mm diameter tool (two flutes, 100% radial immersion with  $x$ -direction feed  $K_t = 700 \text{ N/mm}^2$ ,  $K_r = 0.3$ ).



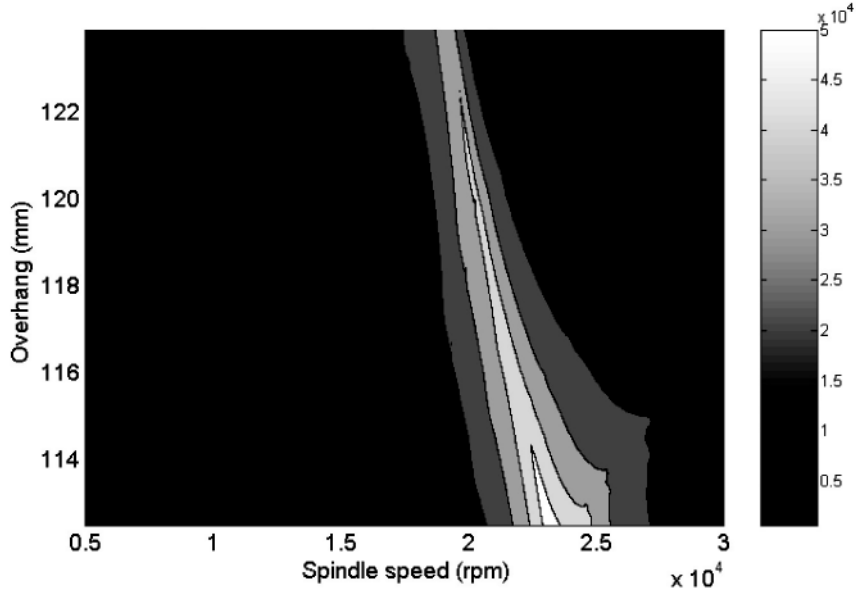


Figure 10. Altintas and Budak formulation MRP contour plot for 12.7 mm diameter tool (two flutes, 100% radial immersion with  $x$ -direction feed,  $K_t = 700 \text{ Nc/mm}^2$ ,  $K_r = 0.3$ , feed per tooth = 0.1 mm). Gray-scale units are  $\text{mm}^3/\text{min}$ .

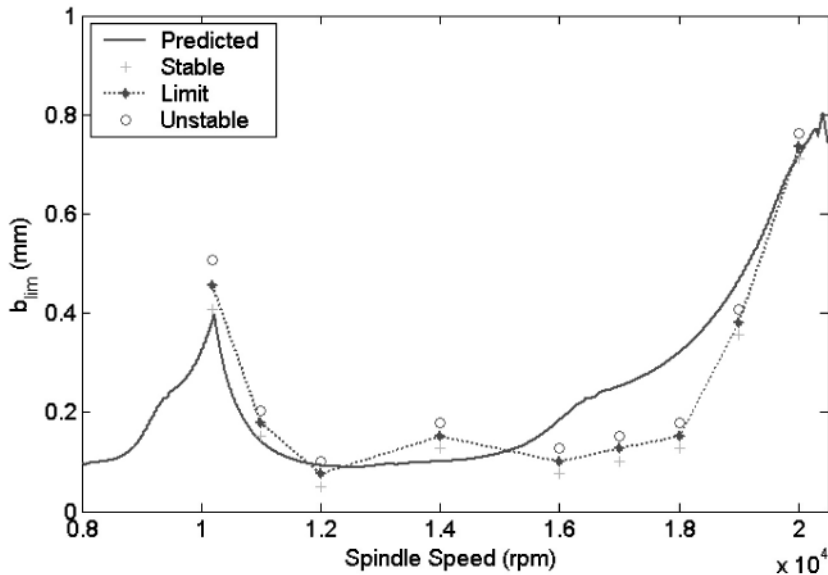


Figure 11. Altintas and Budak formulation 2-D stability lobes and experimental data for 12.7 mm diameter tool with 121.0 mm overhang (two flutes, 100% radial immersion with  $x$ -direction feed,  $K_t = 700 \text{ N/mm}^2$ ,  $K_r = 0.3$ ).



## CONCLUSIONS

In this work, we have demonstrated 3-D stability surfaces which provide the allowable chip width (or axial depth of cut in peripheral milling) as a function of both spindle speed and tool overhang length. Variations in the tool point frequency response as a function of tool overhang length were determined using Receptance Coupling Substructure Analysis (RCSA), an analytic method that couples a model of the tool to a measurement of the holder/spindle through empirically-determined connection parameters. Stability diagrams using the Altintas and Budak formulation were calculated using the RCSA predictions and a contour map was presented to show the variation in achievable material removal rates with overhang length and spindle speed. Milling experiments were also completed to compare stability predictions, using the RCSA frequency response predictions as input, to actual stability limits for the modeled system.

## ACKNOWLEDGMENTS

The authors gratefully acknowledge partial financial support for this research from the National Science Foundation (DMII-0238019) and Office of Naval Research (2003 Young Investigator Program). The authors also wish to recognize Dr. M. Davies, University of North Carolina-Charlotte, and Dr. R. Ivester, National Institute of Standards and Technology, for technical suggestions; K. Medicus, University of North Carolina-Charlotte for help in completing the machining tests; and Dr. T. Insperger, Budapest University of Technology and Economics, for providing the F.W. Taylor quote.

## REFERENCES

- Altintas, Y. (2001). Analytical prediction of three dimensional chatter stability in milling. Japan society of mechanical engineers. International journal series C: mechanical systems. *Machine Elements and Manufacturing* 44(3):717–723.
- Altintas, Y., Budak, E. (1995). Analytical prediction of stability lobes in milling. *Annals of the CIRP* 44(1):357–362.
- Arnold, R. N. (1946). The mechanism of tool vibration in the cutting of steel. *Proceedings of the Institution of Mechanical Engineers* 154(4):261–284.
- Balachandran, B. (2001). Non-linear dynamics of milling process. *Philosophical Transactions of the Royal Society of London A* 359:793–819.
- Bayly, P., Schmitz, T., Peters, D., Mann, B., Stépán, G., Insperger, T. (2002). Effects of radial immersion and cutting direction on chatter instability in end-milling. In: Proceedings of ASME International Mechanical Engineering Congress and Exposition. New Orleans, LA, IMECE2002-34116.



- Bayly, P. V., Halley, J. E., Mann, B. P., Davies, M. A. (2001). Stability of interrupted cutting by temporal finite element analysis. In: Proceedings of the 18th Biennial Conference on Mechanical Vibration and Noise. DETC2001/VIB-21581, ASME Design Engineering Technical Conferences. Pittsburgh: PA, September 9–13.
- Bishop, R. E. D., Johnson, D. C. (1960). *The Mechanics of Vibration*. Cambridge, UK: Cambridge University Press.
- Budak, E., Altintas, Y. (1998). Analytical prediction of chatter stability conditions for multi-degree of freedom systems in milling, Part I: modeling, Part II: applications. *Journal of Dynamic Systems, Measurement and Control* 120:22–36.
- Corpus, W. T., Endres, W. J. (year). A high order solution for the added stability lobes in intermittent machining. In: Proceeding of the Symposium on Machining Processes. Orlando, FL, 871–878, MED-11.
- Davies, M., Balachandran, B. (2000). Impact dynamics in milling of thin-walled structures. *Nonlinear Dynamics* 22:375–392.
- Davies, M., Dutterer, B., Pratt, J., Schaut, A. (1998). On the dynamics of high-speed milling with long, slender endmills. *Annals of the CIRP* 47(1):55–60.
- Den Hartog, J. P. (1956). *Mechanical Vibrations*. 4th ed. New York: McGraw-Hill Book Co., Inc.
- Duncan, W. J. (1947). *Mechanical Admittances and their Applications to Oscillation Problems*. London: Ministry of Supply, Aeronautical Research Council Reports and Memoranda No. 2000, His Majesty's Stationery Office.
- Ferreira, J., Ewins, D. (1995). Nonlinear receptance coupling approach based on describing functions. In: Proceedings of the 14th International Modal Analysis Conference. Dearborn, MI, 1034–1040.
- Fofana, M., Bukkapatnam, S. (2001). A nonlinear model of machining dynamics. In: Proceedings of the 18th Biennial Conference on Mechanical Vibration and Noise, ASME, Design Engineering Technical Conferences. Pittsburgh, PA, September, 9–13; DETC2001/VIB-21582.
- Grabec, I. (1988). Chaotic dynamics of the cutting process. *International Journal of Machine Tools and Manufacture* 28:19–32.
- Hanna, N. H., Tobias, S. A. (1974). A Theory of nonlinear regenerative chatter. *Journal of Engineering for Industry* 96:247–255.  
<http://www.schunk-usa.com/hmhs/home.html>.
- Inspurger, T., Stépán, G. (2002). Semi-discretization method for delayed systems. *International Journal of Numerical Methods in Engineering* 55(5):503–518.
- Jensen, S., Shin, Y. (1999). Stability analysis in face milling operations, Part 1: theory of stability lobe prediction. *Journal of Manufacturing Science and Engineering* 121(4):600–605.
- Kalmar-Nagy, T., Pratt, J. R., Davies, M. A., Kennedy, M. (1999). Experimental and analytical investigation of the subcritical instability in metal cutting. In: Proceedings of the 17th Biennial Conference on Mechanical Vibration and Noise, ASME Design and Technical Conferences. Las Vegas, NV, September 12–16.
- Kegg, R. L. (1965). Cutting dynamics in machine tool chatter. *Journal of Engineering for Industry* 87(4):464–470.



- Koenisberger, F., Tlustý, J. (1967). *Machine Tool Structures: Stability Against Chatter*. Pergamon Press, Vol. I.
- Merrit, H. (1965). Theory of self-excited machine tool chatter. *Journal of Engineering for Industry* 87(4):447–454.
- Minis, I., Yanushevsky, T., Tembo, R., Hocken, R. (1990). Analysis of linear and nonlinear chatter in milling. *Annals of the CIRP* 39(1):459–462.
- Nayfeh, A. H., Chin, C.-M., Pratt, J. (1997). Applications of perturbation methods to tool chatter dynamics. *Dynamics and Chaos in Manufacturing Processes*. New York: Wiley.
- Pratt, J., Davies, M. A., Evans, C. J., Kennedy, M. (1999). Dynamic interrogation of a basic cutting process. *Annals of the CIRP* 48(1):39–42.
- Roa, B., Shin, Y. C. (1999). A comprehensive dynamic cutting force model of chatter prediction in turning. *International Journal of Machine Tools and Manufacture* 39(10):1631–1654.
- Schmitz, T. (2002). Automatic trimming of machining stability lobes. *International Journal of Machine Tools and Manufacture* 42:1479–1486.
- Schmitz, T., Donaldson, R. (2000). Predicting high-speed machining dynamics by substructure analysis. *Annals of the CIRP* 49(1):303–308.
- Schmitz, T., Davies, M. (2001). Tool point frequency response prediction for high-speed machining by RCSA. *Journal of Manufacturing Science and Engineering* 123:700–707.
- Schmitz, T., Burns, T. (2003). Receptance coupling for high-speed machining dynamics prediction. In: Proceedings of the 21st International Modal Analysis Conference. Kissimmee, FL, February 3–6 (on CD).
- Schmitz, T., Davies, M., Medicus, K., Snyder, J. (2001). Improving high-speed machining material removal rates by rapid dynamic analysis. *Annals of the CIRP* 50(1):263–268.
- Shridar, R., Hohn, R. E., Long, G. W. (1968). A stability algorithm for the general milling process. *Journal of Engineering for Industry* 90:330.
- Smith, S., Tlustý, J. (1990). Update on high-speed milling dynamics. *Journal of Engineering for Industry* 112:142–149.
- Smith, S., Tlustý, J. (1991). An overview of modeling and simulation of the milling process. *Journal of Engineering for Industry* 113:169–175.
- Smith, S., Tlustý, J. (1993). Efficient simulation programs for chatter in milling. *Annals of the CIRP* 42(1):463–466.
- Smith, S., Winfough, W., Halley, J. (1998). The effect of tool length on stable metal removal rate in high-speed milling. *Annals of the CIRP* 47(1):307–310.
- Smith, S., Jacobs, T. P., Halley, J. (1999). The effect of drawbar force on metal removal rate in milling. *Annals of the CIRP* 48(1):293–296.
- Stépán, G. (1989). *Retarded Dynamical Systems: Stability and Characteristic Functions*. UK: Longman, Harlow.
- Stépán, G., Kalmar-Nagy, T. (1997). Nonlinear regenerative machine tool vibrations. In: Proceedings of the 16th Biennial Conference on Mechanical Vibration and Noise, ASME, Design Engineering Technical Conferences. Sacramento, CA, September, 14–17; DETC97/VIB-4021.
- Taylor, F. W. (1907). On the art of cutting metals. *Transactions of ASME* 28:31–350.





### Tool Length-Dependent Stability Surfaces

397

- Thusty, J. (1985). Dynamics of high-speed milling. In: King, R. I., ed. *Handbook of High-Speed Machining Technology*. New York: Chapman and Hall, 48–153.
- Thusty, J., Poloczek, M. (1963). The stability of the machine-tool against self-excited vibration in machining. In: Proceedings of the International Research in Production Engineering Conference. Pittsburgh, PA, New York: ASME, 465.
- Thusty, J., Zaton, W., Ismail, F. (1983). Stability lobes in milling. *Annals of the CIRP* 32(1):309–313.
- Thusty, J., Smith, S., Winfough, W. (1996). Techniques for the use of long slender end mills in high-speed machining. *Annals of the CIRP* 45(1):393–396.
- Tobias, S. A. (1965). *Machine-Tool Vibration*. Glasgow, Scotland: Blackie and Sons Ltd.
- Tobias, S. A., Fishwick, W. (1958a). The chatter of lathe tools under orthogonal cutting conditions. *Transactions of the ASME* 80:1079.
- Tobias, S. A., Fishwick, W. (1958b). Theory of regenerative machine tool chatter. *The Engineer*. 205.
- Trent, E. M., Wright, P. K. (2000). *Metal Cutting*. 4th ed. Table 7.2. Woburn, MA: Butterworth-Heinemann.



## **Request Permission or Order Reprints Instantly!**

Interested in copying and sharing this article? In most cases, U.S. Copyright Law requires that you get permission from the article's rightsholder before using copyrighted content.

All information and materials found in this article, including but not limited to text, trademarks, patents, logos, graphics and images (the "Materials"), are the copyrighted works and other forms of intellectual property of Marcel Dekker, Inc., or its licensors. All rights not expressly granted are reserved.

Get permission to lawfully reproduce and distribute the Materials or order reprints quickly and painlessly. Simply click on the "Request Permission/Order Reprints" link below and follow the instructions. Visit the [U.S. Copyright Office](#) for information on Fair Use limitations of U.S. copyright law. Please refer to The Association of American Publishers' (AAP) website for guidelines on [Fair Use in the Classroom](#).

The Materials are for your personal use only and cannot be reformatted, reposted, resold or distributed by electronic means or otherwise without permission from Marcel Dekker, Inc. Marcel Dekker, Inc. grants you the limited right to display the Materials only on your personal computer or personal wireless device, and to copy and download single copies of such Materials provided that any copyright, trademark or other notice appearing on such Materials is also retained by, displayed, copied or downloaded as part of the Materials and is not removed or obscured, and provided you do not edit, modify, alter or enhance the Materials. Please refer to our [Website User Agreement](#) for more details.

### **[Request Permission/Order Reprints](#)**

Reprints of this article can also be ordered at

<http://www.dekker.com/servlet/product/DOI/101081MST200038989>